drones

MDPI

Article

Modeling Analysis for Downlink RIS-UAV-Assisted NOMA over Air-to-Ground Line-of-Sight Rician Channels

Suoping Li [1,*], Xiangyu Liu [1,*], Jaafar Gaber [2] and Guodong Pan [1]

[1] School of Science, Lanzhou University of Technology, Lanzhou 730050, China; id_pgd@163.com
[2] Department of Computer Science and Computer Engineering, the University of Technology of Belfort-Montbéliard, 90010 Belfort, France; gaber@utbm.fr
* Correspondence: lsuop@lut.edu.cn (S.L.); xylauptcss@163.com (X.L.)

Abstract: This paper proposes a drone-assisted NOMA communication system equipped with a reconfigurable intelligent surface (RIS). Given the Line-of-Sight nature of the Air-to-Ground link, a more realistic Rician fading environment is chosen for the study of system performance. The user's outage performance and secrecy outage probability of the RIS-UAV-assisted NOMA downlink communication under the Rician channels are investigated. Jointly considering the Line-of-Sight and Non-Line-of-Sight links, the closed-form expressions of each user's outage probability are derived by approximating the composite channels as Rician distributions to characterize the channel coefficients of the system's links. Considering the physical layer security in the presence of the eavesdropper, the secrecy outage probability of two users is further studied. The relationship between the system outage performance and the Rician factor of the channel, the number of RIS elements, and other factors are analyzed. The results of this study show that compared with Rayleigh fading, the Rician fading is more practical with the actual Air-to-Ground links; the user's outage probability and the secrecy outage probability are lower over the Rician channels. The number of RIS elements and the power allocation factor by the base station for the users are inversely proportional to the user's outage probability, and RIS element number, path loss index, and distance factor also have a greater impact on the outage probability. Compared with OMA, NOMA has a certain enhancement to the system performance.

Keywords: unmanned aerial vehicle; reconfigurable intelligent surface; non-orthogonal multiple access; outage probability; physical layer security; Rician fading

Citation: Li, S.; Liu, X.; Gaber, J.; Pan, G. Modeling Analysis for Downlink RIS-UAV-Assisted NOMA over Air-to-Ground Line-of-Sight Rician Channels. *Drones* **2024**, *8*, 659. https://doi.org/10.3390/drones8110659

Academic Editors: Sai Huang, Weiwei Jiang, Yafeng Zhan, Ray E. Sheriff and Zhiyong Feng

Received: 21 September 2024
Revised: 3 November 2024
Accepted: 5 November 2024
Published: 8 November 2024

1. Introduction

In 2021, the Ministry of Industry and Information Technology of China issued the "14th Five-Year Plan" for the Development of the Information and Communication Technology (ICT) Industry, proposing to promote the 6th Generation (6G) Wireless Systems mobile communication core technology research and development and to build an integration network of space, air, earth, and sea. The 6G network is an effective integration of the 5G network, satellite communication network, and deep-sea ocean network [1–3]. The satellite communication network covers various fields such as communication, navigation, remote sensing, and telemetry and realizes integrated global connectivity between space, air, earth, and sea. The space–air–earth–sea integration network will optimize the infrastructure in all spatial areas and achieve full coverage of elements. As shown in Figure 1, an information integration network of space–air–earth–sea mentioned above is given. When the ground communication infrastructure is damaged or unavailable, the UAV can serve as an aerial relay to provide a connection with the terminals, constituting an Air-to-Ground communication link [4–6].

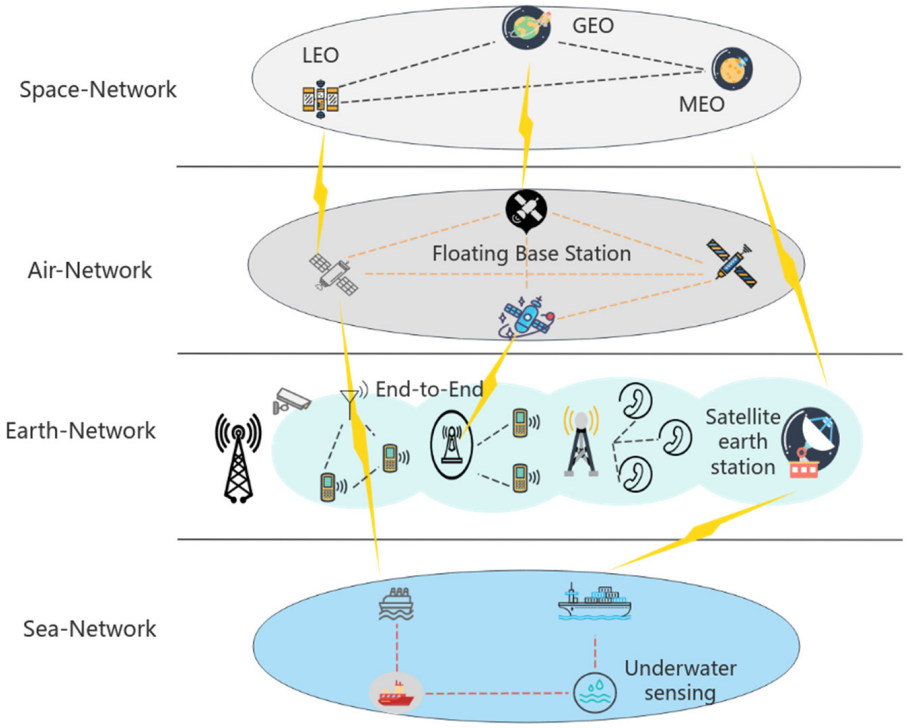

Figure 1. The space–air–earth–sea integration network.

Unmanned Aerial Vehicle (UAV) mobile communication technology is a key technology for the construction of space, air, earth, and sea integration networks and has become emerging hot research in wireless communication with its advantages of deployment flexibility, Line-of-Sight (LoS) transmission, low cost, and wide coverage. Its inherent mobility and flexibility can be deployed on-demand in a timely manner and provide higher wireless capacity, higher reliability, and higher coverage for the systems, which have extremely high potential application value [7]. Reconfigurable Intelligent Surface (RIS) has become a promising research direction for future auxiliary wireless communications due to its small number of active or passive device design concepts, low cost, low power consumption, low complexity, and accessibility of deployment [8,9]. RIS only reflects the wireless propagation signals intelligently, which requires less energy and, at the same time, improves the wireless propagation channel environment, reduces the loss of wireless spectrum, and thus improves the spectral efficiency and energy efficiency. As an energy-constrained system, there exists a shortage of UAV communication in extent. Therefore, we can consider the wireless communication system that deploys RIS on the UAV, which is able to enhance the performance of the communication system by optimizing the phase shift of RIS at the same time and flexibly deploying the location of the UAV. As a promising technology in 5G, Non-Orthogonal Multiple Access (NOMA) can increase the capacity of the wireless communication system, allowing multiple users to share the same resources, and has the advantages of large-scale connectivity, low latency, high spectral efficiency, etc. NOMA can, therefore, also integrate with other technologies to obtain better spectrum efficiency, such as large-scale Multiple-Input Multiple-Output (MIMO), low latency, and high spectrum efficiency, millimeter wave, Simultaneous Wireless Information and Power Transfer (SWIPT), and UAV communication. Due to the strong compatibility of RIS, NOMA technology can be applied to the RIS-UAV communication network to further improve the performance of the communication system.

In order to facilitate the analysis, most of the existing related researches focus on the Rayleigh fading channels of Non-Line-of-Sight (NLoS) links, but according to the design of the RIS principle and the Air-to-Ground links of UAV-assisted communication, it is verified that it can be better applied to the Rician fading environment of LoS links, so it

can be more in line with the practical application to explore the auxiliary effect of RIS-UAV communication systems over the Rician channel. Ref. [10] investigated the safety outage problem of UAV as an auxiliary relay under the Rician fading channel and jointly designed the beamforming and UAV's flight trajectory to improve the system's security. Ref. [11] investigated the time-varying beamforming and power allocation of the full-duplex UAV relay under Rician fading channels to improve the system performance. Refs. [12,13] explored the spectral efficiency and outage performance of RIS systems with continuous phase shifts by analyzing the Rayleigh channel distribution of the communication system. Refs. [14,15] analyzed the outage probability, secrecy outage probability, and traversal security rate under Rayleigh channels for RIS-assisted communication systems with security constraints; ref. [16] analyzed the outage probability and traversal security rate under the presence of eavesdroppers, analyzed the channel distribution characteristics of the eavesdropping channel by using the central limit theorem, and explored the relationship between the traversal security rate and the number of RIS reflection elements when it approaches infinity. Some researchers have also investigated the outage probability and traversal rate of the system model under the Rician fading channels [17,18], ref. [19] analyzed the mean square value of the composite channel by splitting the LoS component in the Rician channel, and ref. [20] obtained the corresponding variance to the composite channel when the RIS component approached infinity by dissolving the real and imaginary parts of the Rayleigh composite channel.

The high spectrum efficiency of NOMA has received much attention. Due to the broadcast nature of signal propagation and the vulnerability of eavesdropping attacks by illegal users, there have been many studies on NOMA technology and its application in Physical Layer Secure (PLS) communications [21,22]. Ref. [23] evaluated the confidentiality performance of a large-scale NOMA downlink system in the presence of eavesdroppers; ref. [24] proposed a millimeter-wave based on the NOMA confidential beamforming scheme and gave the corresponding closed-form expressions for the confidential outage probability of paired users. Ref. [25] considered internal and external eavesdropping scenarios as well as imperfect successive interference cancellation and perfect interference cancellation, respectively, to provide a secure communication solution for the RIS-assisted NOMA system, which verifies that NOMA has better confidentiality performance for system security than OMA and that the number of RIS elements is proportional to the security of the system to a certain degree. Ref. [26] considered the scenario where the direct and reflective links of the BTS users and the BTS-RIS users exist simultaneously by designing the RIS to increase the signal reception strength of the NOMA near users and further deduce the closed-form expression for the system outage probability and traversal capacity. The interference noise method is proposed to improve the system security and confidentiality, and the security outage probability of the system is deduced in the presence of eavesdroppers in [27].

To satisfy the Air-to-Ground LoS link that is more in line with the actual situation and to improve the overall communication performance of the system, this paper considers exploring the RIS-UAV-assisted NOMA communication system under the Rician fading channel environment, and the main work is as follows:

- Different from other studies, on the basis of researching the influence of RIS on the communication system under the circumstance of Rician fading, this paper, combined with the development of space–air–earth–sea integration information network, introduced NOMA technology to further improve the system performance in the Air-to-Ground LoS link scenario of the UAV cooperative communication and considered the user's communication security performance under the presence of the eavesdropper.
- For the NOMA downlink communication system assisted by RIS-UAV over Rician fading channels, this paper systematically analyzes the distribution model and obtains the corresponding channel cumulative distribution function.

- Explore the outage performance of two users in the NOMA downlink communication systems, and the user's information transmission secrecy outage probability has been studied in the presence of the illegal eavesdropper based on Wiener's eavesdropping theory.
- Through numerical simulation, then explore the effect of the Rician factor, the number of RIS elements, etc., on the outage performance of the system, and compared with the OMA system, the effect of NOMA technology on the performance of the communication system is verified.

2. System Model

As an energy-constrained system of UAV communication, RIS can be deployed on UAV to improve the performance of the communication system. In practical applications, when there is a large barrier between the base station and the target user that affects the communication, a RIS-UAV can be considered and deployed at a certain location for auxiliary communication. Thus, considering a dedicated UAV carrying uniform rectangular array (URA) RIS-assisted NOMA downlink communication system in Figure 2, which includes a base station (BS), a RIS-UAV, legitimate users U_1 and U_2, and an illegal eavesdropping user U_e (User Eve), and all the nodes are equipped with a single antenna and communicate in half-duplex mode. Firstly, the base station transmits the superimposed NOMA signal to the legitimate users. Since there exist obstacles between the base station and the users, only the links from the base station to the RIS-UAV and from the RIS-UAV to the users are considered. The signal is reflected to the legitimate users on the ground through the RIS-UAV, which is equipped with a reconfigurable intelligent surface. RIS reflects the signal and transmits it to two legitimate users, respectively. The user decodes the signal through the NOMA communication principle and SIC process to obtain the required information. At the same time, an illegal user U_e eavesdrops on the information transmitted between the base station and users to destroy the communication security.

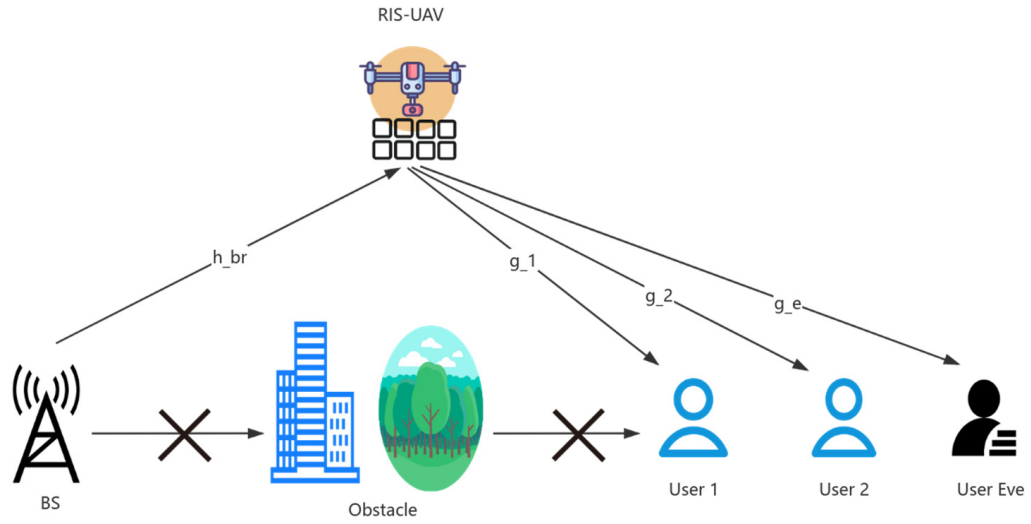

Figure 2. System model of RIS-UAV-assisted NOMA downlink communication networks.

For the convenience of research, it is assumed that the UAV is at a certain location and the coordinates of the base station, the UAV, the users, and the eavesdropper are $w_B(x_B, y_B, 0)$, $w_R(x_R, y_R, h)$, $w_k(x_k, y_k, 0)$, respectively, where $\forall k \in \{1, 2, e\}$. Supposing that each channel in the communication system considered in this paper has statistical Channel State Information (CSI), the RIS is equipped with M elements, respectively. The diagonal matrix $\Phi = diag\{\varphi_1, \varphi_2, \cdots \varphi_M\}$ and $\varphi_m = a_r e^{j\theta_m}$ is the diagonal matrix constituent of RIS, where a_r is the amplitude reflection coefficient, θ_m is the phase shift reflection coefficient. In general, in the conventional passive RIS of this paper, the $a_r = 1$. There are Line-of-Sight links between the base station to the RIS-UAV and the RIS-UAV to the user, so each channel is modeled as a Rician channel.

The channel between the BS and the RIS-UAV is denoted by $h_{b,r} \in C^{M\times 1}$ and the channel between the RIS-UAV and the user is denoted by $g_k \in C^{M\times 1}$. Each channel is modeled as follows:

$$h_{b,r} = \sqrt{{d_{b,r}}^{-\alpha} \cdot h_0}\left(\sqrt{\frac{R_1}{R_1+1}}{h_{b,r}}^{LOS} + \sqrt{\frac{1}{R_1+1}}{h_{b,r}}^{NLOS}\right) \tag{1}$$

$$g_k = \sqrt{{d_{r,k}}^{-\beta} \cdot h_0}\left(\sqrt{\frac{R_2}{R_2+1}}{g_k}^{LOS} + \sqrt{\frac{1}{R_2+1}}{g_k}^{NLOS}\right) \tag{2}$$

where $d_{b,r}$ and $d_{r,k}$ are the distances from the base station to the RIS-UAV center and from the RIS-UAV center to the user, respectively. α is the path loss index from the base station to the RIS-UAV; β is the path loss index of the RIS-UAV to the user. h_0 is the path loss exponent per unit of distance, R_1 and R_2 are the Rician channel factors of the two links, respectively. ${h_{b,r}}^{LOS}$ and ${g_k}^{LOS}$ are the LoS components, ${h_{b,r}}^{NLOS}$ and ${g_k}^{NLOS}$ are the NLoS components that obey a complex Gaussian distribution with mean 0 and variance 1, i.e., ${h_{b,r}}^{NLOS} \sim CN(0,1)$, ${g_k}^{NLOS} \sim CN(0,1)$.

According to the NOMA transmission power domain mode and successive interference cancellation (SIC) process, the signal at the transmitter and receiver ends expressions are established. Therefore, the base station transmits the superimposed signal of two users by using appropriate power coefficients based on the channel conditions:

$$s = \sqrt{\alpha_1 P}s_1 + \sqrt{\alpha_2 P}s_2 \tag{3}$$

where P is the transmitting power of the base station, $\alpha_1 + \alpha_2 = 1$ based on the power allocation principle of the power domain NOMA.

For the receiving end, the signal received by user 1, user 2, and the eavesdropper is as follows:

$$y_k = g_k^H \Phi h_{b,r} s + n_k \tag{4}$$

where $n_k \sim CN(0, {\sigma_k}^2)$ is the additive white Gaussian noise (AWGN). For the convenience, the equivalent noise power, i.e., $\sigma_1^2 = \sigma_2^2 = \sigma_k^2 = \sigma_0^2$ are used in this paper.

Since the NOMA system, the information rate of each user after the SIC process is considered. Due to the closer distance of U_1, it is assumed that the channel condition of U_1 is better than that of U_2. Then, according to the SIC decoding order, it is to demodulate in the order of which the channel gain increases. For U_2, the information of U_1 is treated as noise to decode its own information directly. For U_1, because of the larger channel gain, when decoding the information, it needs to decode U_2's information first, then decode its own signal after removing U_2's information. Therefore, for the decoded information at the two legitimate users, the SINR (Signal-to-Noise Ratio) is as follows:

$$\gamma_{1\to 1} = \frac{\left|g_1^H \Phi h_{b,r}\right|^2 \times \alpha_1 P}{{\sigma_0}^2} \tag{5}$$

$$\gamma_{2\to 2} = \frac{\left|g_2^H \Phi h_{b,r}\right|^2 \times \alpha_2 P}{\left|g_2^H \Phi h_{b,r}\right|^2 \times \alpha_1 P + {\sigma_0}^2} \tag{6}$$

$$\gamma_{1\to 2} = \frac{\left|g_1^H \Phi h_{b,r}\right|^2 \times \alpha_2 P}{\left|g_1^H \Phi h_{b,r}\right|^2 \times \alpha_1 P + {\sigma_0}^2} \tag{7}$$

Therefore, the information decoding rates for the two users are as follows:

$$Ru_1 = R_{1,1} = \log_2\left(1 + \frac{\left|g_1^H \Phi h_{b,r}\right|^2 \times \alpha_1 P}{{\sigma_0}^2}\right) \tag{8}$$

$$Ru_2 = \min(R_{1,2}, R_{2,2}) \tag{9}$$

where

$$R_{1,2} = \log_2(1 + \frac{\left|g_1^H \Phi h_{b,r}\right|^2 \times \alpha_2 P}{\left|g_1^H \Phi h_{b,r}\right|^2 \times \alpha_1 P + {\sigma_0}^2}) \tag{10}$$

$$R_{2,2} = \log_2(1 + \frac{\left|g_2^H \Phi h_{b,r}\right|^2 \times \alpha_2 P}{\left|g_2^H \Phi h_{b,r}\right|^2 \times \alpha_1 P + {\sigma_0}^2}) \tag{11}$$

To ensure the SIC, let $R_{1,2} \geq R_{2,2}$, therefore:

$$Ru_1 = \log_2(1 + \frac{\left|g_1^H \Phi h_{b,r}\right|^2 \times \alpha_1 P}{{\sigma_0}^2}) \tag{12}$$

$$Ru_2 = \log_2(1 + \frac{\left|g_2^H \Phi h_{b,r}\right|^2 \times \alpha_2 P}{\left|g_2^H \Phi h_{b,r}\right|^2 \times \alpha_1 P + {\sigma_0}^2}) \tag{13}$$

When the system transmits information in OMA mode, the information rate of the two users are as follows:

$$R_{u1}^{oma} = \eta \log_2(1 + \frac{\left|g_1^H \Phi h_{b,r}\right|^2 \times \alpha_1 P}{\eta {\sigma_0}^2}) \tag{14}$$

$$R_{u2}^{oma} = (1 - \eta) \log_2(1 + \frac{\left|g_2^H \Phi h_{b,r}\right|^2 \times \alpha_2 P}{(1 - \eta) {\sigma_0}^2}) \tag{15}$$

In the NOMA system, the two users can use 1 Hz bandwidth simultaneously; in the OMA system, user 1 uses η Hz bandwidth and user 2 uses $(1 - \eta)$ Hz bandwidth. For convenience of subsequent calculation, it is assumed that the two users use the same bandwidth, that is $\eta = \frac{1}{2}$. The subsequent research and analysis are still dominated by NOMA.

For the eavesdropper user U_e, considering the worst case that the eavesdropper can perform complete interference cancellation for both users' messages [28–30]. Based on the SIC and the RIS reflected incident signal, the eavesdropper's SINR can be derived:

$$\gamma_{e \to 1} = \frac{\left|g_e^H \Phi h_{b,r}\right|^2 \times \alpha_1 P}{\sigma_0^2} \tag{16}$$

$$\gamma_{e \to 2} = \frac{\left|g_e^H \Phi h_{b,r}\right|^2 \times \alpha_2 P}{\sigma_0^2} \tag{17}$$

Thus, the rate of information eavesdropping at the eavesdropper for U_1 and U_2 are, respectively:

$$R_{e1} = \log_2(1 + \frac{\left|g_e^H \Phi h_{b,r}\right|^2 \times \alpha_1 P}{\sigma_0^2}) \tag{18}$$

$$R_{e2} = \log_2(1 + \frac{\left|g_e^H \Phi h_{b,r}\right|^2 \times \alpha_2 P}{\sigma_0^2}) \tag{19}$$

According to Wyner's eavesdropping theory, the eavesdropper's secrecy rate for the two users can be expressed, respectively:

$$\begin{cases} R_{s1} = (R_1 - R_{e1})^+ \\ R_{s2} = (R_2 - R_{e2})^+ \end{cases} \tag{20}$$

3. Problem Formulation and Performance Analysis

3.1. Problem Formulation

This section addresses the outage performance of the RIS-UAV-assisted NOMA downlink system with statistical CSI for the system under Rician fading. Since the per-element distance of the RIS is small compared with the distance between the base station, the RIS,

and users that can be described as far-field communication, the impact of the orientation and size of the RIS on the path loss model can be neglected. However, since the small wavelength, the distance from different elements of the RIS to the base station and the user cannot be neglected. Then, the channels from the base station to the $m-th$ element of the RIS and from the $m-th$ element of the RIS to the user under the Rician channel are modeled as:

$$h_{b,r(m)} = \sqrt{{d_{b,r}}^{-\alpha} \cdot h_0}\left(\sqrt{\frac{R_1}{R_1+1}}{h_{b,r(m)}}^{LOS} + \sqrt{\frac{1}{R_1+1}}{h_{b,r(m)}}^{NLOS}\right) \tag{21}$$

$$g_{k(m)} = \sqrt{{d_{r,k}}^{-\beta} \cdot h_0}\left(\sqrt{\frac{R_{2,k}}{R_{2,k}+1}}{g_{k(m)}}^{LOS} + \sqrt{\frac{1}{R_{2,k}+1}}{g_{k(m)}}^{NLOS}\right) \tag{22}$$

where $R_{2,k}$ indicates the Rician factor of the channel between the RIS-UAV and the user, where $k \in (1,2,e)$. ${h_{b,r(m)}}^{LOS} = e^{-j\frac{2\pi}{\lambda}a_m}$, ${g_{k(m)}}^{LOS} = e^{-j\frac{2\pi}{\lambda}b_m}$, a_m and b_m are the distances from the base station to the $m-th$ RIS element and from the $m-th$ RIS element to the users, respectively.

When the reachable rate is lower than the target rate, we consider an interruption to be occurred. For U_1, the outage probability is as follows:

$$\begin{aligned} P_{out1} &= \Pr\left\{\log_2(1+\gamma_1) < \widetilde{R}_1\right\} = \Pr\{\log_2(1+\frac{\left|g_1^H \Phi h_{b,r}\right|^2 \times \alpha_1 P}{\sigma_0^2}) < \widetilde{R}_1\} \\ &= \Pr\{\frac{\left|\sum_{m=1}^{M} g_{1(m)} e^{j\theta_m} h_{b,r(m)}\right|^2 \times \alpha_1 P}{\sigma_0^2} < \gamma_{th1}\} = \Pr\{|\sum_{m=1}^{M} g_{1(m)} e^{j\theta_m} h_{b,r(m)}|^2 < \frac{\gamma_{th1}}{\alpha_1 \rho}\} \\ &= \Pr\{|H_1|^2 < \frac{\gamma_{th1}}{\alpha_1 \rho}\} \end{aligned} \tag{23}$$

where $\widetilde{R}_1$ denotes the target rate of U_1, $\gamma_{th1} = 2^{\widetilde{R}_1} - 1$. $\rho = \frac{P}{\sigma_0^2}$ denotes the base station transmitting Signal-to-Noise Ratio(SNR). $H_1 = \sum_{m=1}^{M} g_{1(m)} e^{j\theta_m} h_{b,r(m)}$ denotes the equivalent channel of which the signal arrives at user 1 from the base station through the RIS.

Similarly, for U_2, its outage probability is as follows:

$$\begin{aligned} P_{out2} &= \Pr\left\{\log_2(1+\gamma_2) < \widetilde{R}_2\right\} \\ &= \Pr\{\log_2(1+\frac{\left|g_{2(m)}^H \Phi h_{b,r(m)}\right|^2 \times \alpha_2 P}{\left|g_{2(m)}^H \Phi h_{b,r(m)}\right|^2 \times \alpha_1 P + \sigma_0^2}) < \widetilde{R}_2\} \\ &= \Pr\left\{\frac{\left|\sum_{m=1}^{M} g_{2(m)} e^{j\theta_m} h_{b,r(m)}\right|^2 \times \alpha_2 P}{\left|\sum_{m=1}^{M} g_{2(m)} e^{j\theta_m} h_{b,r(m)}\right|^2 \times \alpha_1 P + \sigma_0^2} < \gamma_{th2}\right\} \\ &= \Pr\left\{\frac{\left|\sum_{m=1}^{M} g_{2(m)} e^{j\theta_m} h_{b,r(m)}\right|^2 \times \alpha_2 \rho}{\left|\sum_{m=1}^{M} g_{2(m)} e^{j\theta_m} h_{b,r(m)}\right|^2 \times \alpha_1 \rho + 1} < \gamma_{th2}\right\} \\ &= \Pr\left\{\left|\sum_{m=1}^{M} g_{2(m)} e^{j\theta_m} h_{b,r(m)}\right|^2 \times \alpha_2 \rho < \gamma_{th2} \times \left|\sum_{m=1}^{M} g_{2(m)} e^{j\theta_m} h_{b,r(m)}\right|^2 \times \alpha_1 \rho + \gamma_{th2}\right\} \\ &= \Pr\left\{\left|\sum_{m=1}^{M} g_{2(m)} e^{j\theta_m} h_{b,r(m)}\right|^2 \times (\alpha_2 \rho - \gamma_{th2} \times \alpha_1 \rho) < \gamma_{th2}\right\} \\ &= \Pr\left\{\left|\sum_{m=1}^{M} g_{2(m)} e^{j\theta_m} h_{b,r(m)}\right|^2 < \frac{\gamma_{th2}}{(\alpha_2 \rho - \gamma_{th2} \times \alpha_1 \rho)}\right\} \\ &= \Pr\left\{|H_2|^2 < \frac{\gamma_{th2}}{(\alpha_2 \rho - \gamma_{th2} \times \alpha_1 \rho)}\right\} \end{aligned} \tag{24}$$

where $\widetilde{R}_2$ denotes the target rate of U_2, $\gamma_{th2} = 2^{\widetilde{R}_2} - 1$. $H_2 = \sum_{m=1}^{M} g_{2(m)} e^{j\theta_m} h_{b,r(m)}$ denotes the equivalent channel of which the signal arrives at user 2 from the base station through the RIS.

3.2. Outage Performance Analysis

To derive the outage probability for each user and the information secrecy outage probability in the next part, the channels' distribution and the distribution of signal-to-noise ratios for the two users and the eavesdropper need to be calculated. Here, the channel distribution of user 1 and its SNR distribution as well as the eavesdropper's information secrecy outage probability for user 1, are analyzed in detail.

Since the channel consists of LoS and NLoS parts:

$$H_1 = \sum_{m=1}^{M} g_{1(m)} e^{j\theta_m} h_{b,r(m)} = H_1^{LoS} + H_1^{NLoS} \tag{25}$$

According to $h_{b,r(m)}$ and $g_{1(m)}$, we can obtain:

$$H_1^{LoS} = h_0 \sqrt{d_{b,r}^{-\alpha} \times d_{r,1}^{-\beta}} \sqrt{\frac{R_1 \times R_{2,1}}{(R_1+1)(R_{2,1}+1)}} \sum_{m=1}^{M} e^{j(\theta_m - \frac{2\pi}{\lambda}(a_m + b_m))} \tag{26}$$

$$\begin{aligned} H_1^{NLoS} = \sum_{m=1}^{M} e^{j\theta_m} h_0 \sqrt{d_{b,r}^{-\alpha} \times d_{r,1}^{-\beta}} \Bigg\{ \sqrt{\frac{R_1}{(R_1+1)(R_{2,1}+1)}} h_{b,r(m)}^{LoS} g_{1(m)}^{NLoS} + \\ \sqrt{\frac{R_2}{(R_1+1)(R_{2,1}+1)}} g_{1(m)}^{LoS} h_{b,r(m)}^{NLoS} + \sqrt{\frac{1}{(R_1+1)(R_{2,1}+1)}} h_{b,r(m)}^{NLoS} g_{1(m)}^{NLoS} \Bigg\} \end{aligned} \tag{27}$$

Since $h_{b,r(m)}^{NLoS}$ and $g_{1(m)}^{NLoS}$ follow the complex Gaussian distribution with mean 0 and variance 1, it can be approximated as a complex Gaussian distribution for the whole H_1^{NLoS}:

$$H_1^{NLoS} \sim CN(0, \frac{M \times h_0^2 \times d_{b,r}^{-\alpha} \times d_{r,1}^{-\beta} (R_1 + R_{2,1} + 1)}{(R_1+1)(R_{2,1}+1)}) \tag{28}$$

For convenience, note $\delta_{nl1}^2 = \frac{M \times h_0^2 \times d_{b,r}^{-\alpha} \times d_{r,1}^{-\beta} (R_1 + R_{2,1} + 1)}{(R_1+1)(R_{2,1}+1)}$.

The channel H_1 can be viewed as a composite channel consisting of a LoS portion and an NLoS portion, thus approximating it as a Rician distribution, where the main signal is H_1^{LoS} and the H_1^{NLoS} is NLoS signal. The sum of power gains on all paths is considered to be 1. The Rician random variable X can be viewed as the arithmetic square root of two mutually independent zero-mean Gaussian random variables, then the random variable $|X|^2$ obeys a non-central chi-square distribution with 2 degrees of freedom, and its corresponding probability density function (PDF) and cumulative distribution function (CDF) are as follows:

$$f_{|X|^2}(x) = (R+1) \exp[-(R + (R+1)x)] I_0(2\sqrt{xR(R+1)}) \tag{29}$$

$$F_{|X|^2}(x) = P\left\{ \left| X \right|^2 \leq x \right\} = 1 - Q_1(\sqrt{2R}, \sqrt{2(1+R)x}) \tag{30}$$

The Rician distribution is usually described by the Rician factor, i.e., $R = \frac{v^2}{2\sigma^2}$, which represents the ratio of the direct signal component power and the scattered signal component power. v denotes the peak amplitude of the LoS signal, σ^2 denotes the signal power; $Q_1(a,b) = \int_b^\infty x \exp(-\frac{x^2+a^2}{2}) I_0(ax) dx$ is the first-order Marcum-Q function, and $I_0(\cdot)$ is the first-type zero-order modified Bessel function.

For the channel H_1 in this paper, v denotes the LoS signal, δ_{nl1}^2 is the power of the scattered component, thus:

$$v = |H_1^{LoS}| = h_0\sqrt{d_{b,r}^{-\alpha} \times d_{r,1}^{-\beta}}\sqrt{\frac{R_1 \times R_{2,1}}{(R_1+1)(R_{2,1}+1)}}|\sum_{m=1}^{M} e^{j(\theta_m - \frac{2\pi}{\lambda}(a_m+b_m))}|$$

For $|H_1|^2$, the corresponding CDF is: $F_{|H_1|^2}(x) = 1 - Q_1(\sqrt{\frac{2}{\delta_{nl}^2}}|H_1^{LoS}|, \sqrt{\frac{2}{\delta_{nl}^2}x})$. Therefore, the outage probability for U_1 is as follows:

$$P_{out1} = 1 - Q_1(\sqrt{\frac{2}{\delta_{nl1}^2}}|H_1^{LoS}|, \sqrt{\frac{2}{\delta_{nl1}^2}} \times \sqrt{\frac{\gamma_{th1}}{\alpha_1\rho}}) \tag{31}$$

Similarly, the outage probability for U_2 can be obtained as:

$$P_{out2} = 1 - Q_1(\sqrt{\frac{2}{\delta_{nl2}^2}}|H_2^{LoS}|, \sqrt{\frac{2}{\delta_{nl2}^2}} \times \sqrt{\frac{\gamma_{th2}}{\alpha_2\rho - \gamma_{th2} \times \alpha_1\rho}}) \tag{32}$$

where $\delta_{nl2}^2 = \frac{M \times h_0^2 \times d_{b,r}^{-\alpha} \times d_{r,2}^{-\beta}(R_1+R_{2,2}+1)}{(R_1+1)(R_{2,2}+1)}$, $|H_2^{LoS}| = h_0\sqrt{d_{b,r}^{-\alpha} \times d_{r,2}^{-\beta}}\sqrt{\frac{R_1 \times R_{2,2}}{(R_1+1)(R_{2,2}+1)}}$ $\left|\sum_{m=1}^{M} e^{j(\theta_m - \frac{2\pi}{\lambda}(a_m+b_m))}\right|$.

3.3. User's Secrecy Outage Performance Analysis

According to Wyner's eavesdropping theory, the eavesdropper eavesdrops on the information of two users, and the rate of information security for each user is as follows:

$$\begin{cases} R_{s1} = (R_1 - R_{e1})^+ = [\log_2(1+\gamma_{1\to1}) - \log_2(1+\gamma_{e\to1})]^+ \\ R_{s2} = (R_2 - R_{e2})^+ = [\log_2(1+\gamma_{2\to2}) - \log_2(1+\gamma_{e\to2})]^+ \end{cases} \tag{33}$$

Therefore, the information secrecy outage probability (SOP) for user 1 is as follows:

$$\begin{aligned} P_{out}^{s1} &= \Pr\left\{R_{s1} < \widetilde{R}_{s1}\right\} = \Pr\left\{\log_2(1+\gamma_{1\to1}) - \log_2(1+\gamma_{e\to1}) < \widetilde{R}_{s1}\right\} \\ &= \Pr\left\{\gamma_{1\to1} < 2^{\widetilde{R}_{s1}}(1+\gamma_{e\to1}) - 1\right\} = \int_0^\infty f_{\gamma_{e\to1}}(x) F_{\gamma_{1\to1}}[2^{\widetilde{R}_{s1}}(1+x) - 1]dx \\ &= \int_0^\infty f_{|H_e|^2}(x) F_{|H_1|^2}(\frac{2^{\widetilde{R}_{S1}}(1+\alpha_1\rho * x) - 1}{\alpha_1\rho})dx \end{aligned} \tag{34}$$

Similarly, the information secrecy outage probability for user 2 can be obtained:

$$\begin{aligned} P_{out}^{s2} &= \Pr\left\{R_{s2} < \widetilde{R}_{s2}\right\} = \Pr\left\{\log_2(1+\gamma_{2\to2}) - \log_2(1+\gamma_{e\to2}) < \widetilde{R}_{s2}\right\} \\ &= \Pr\left\{\frac{1 + \frac{|H_2|^2\alpha_2\rho}{|H_2|^2\alpha_1\rho+1}}{1+|H_{e2}|^2\alpha_2\rho} < 2^{\widetilde{R}_{s2}}\right\} \\ &= \Pr\left\{|H_2|^2\rho(\alpha_1+\alpha_2) + 1 < 2^{\widetilde{R}_{S2}}(1+|H_e|^2\alpha_2\rho)(1+|H_2|^2\alpha_1\rho)\right\} \\ &= \Pr\left\{|H_2|^2 < \frac{2^{\widetilde{R}_{S2}}(1+|H_e|^2\alpha_2\rho) - 1}{\rho(\alpha_1+\alpha_2) - 2^{\widetilde{R}_{S2}}(1+|H_e|^2\alpha_2\rho)\alpha_1\rho}\right\} \\ &= \int_0^\infty f_{|H_e|^2}(x) F_{|H_2|^2}(\frac{2^{\widetilde{R}_{S2}}(1+\alpha_2\rho x) - 1}{\rho(\alpha_1+\alpha_2) - 2^{\widetilde{R}_{S2}}(1+\alpha_2\rho x)\alpha_1\rho})dx \end{aligned} \tag{35}$$

According to Equations (34) and (35), the SOP at the eavesdropper for two NOMA users' information security can be obtained as, respectively:

$$\begin{aligned} P_{s1}^{out} &= \int_0^\infty f_{|H_e|^2}(x) F_{|H_1|^2}\left(\frac{2^{\widetilde{R_{S1}}}(1+\alpha_1\rho * x)-1}{\alpha_1\rho}\right)dx \\ &= \int_0^\infty \left(\frac{\left|H_e^{LoS}\right|^2}{\delta_{nle}^2}+1\right)\exp\left[-\left(\frac{\left|H_e^{LoS}\right|^2}{\delta_{nle}^2}+\left(\frac{\left|H_e^{LoS}\right|^2}{\delta_{nle}^2}+1\right)x\right)\right]* \\ &I_0\left(2\sqrt{x*\frac{\left|H_e^{LoS}\right|^2}{\delta_{nle}^2}\left(\frac{\left|H_e^{LoS}\right|^2}{\delta_{nle}^2}+1\right)}\right)* \\ &\left[1-Q_1\left(\sqrt{2\frac{\left|H_1^{LoS}\right|^2}{\delta_{nl1}^2}},\sqrt{2\left(1+\frac{\left|H_1^{LoS}\right|^2}{\delta_{nl1}^2}\right)}*\sqrt{\frac{2^{\widetilde{R_{s1}}}(1+\alpha_1\rho x)-1}{\alpha_1\rho}}\right)\right]dx \end{aligned} \tag{36}$$

$$\begin{aligned} P_{s2}^{out} &= \int_0^\infty f_{|H_e|^2}(x) F_{|H_2|^2}\left(\frac{2^{\widetilde{R_{S2}}}(1+\alpha_2\rho x)-1}{\rho(\alpha_1+\alpha_2)-2^{\widetilde{R_{S2}}}(1+\alpha_2\rho x)\alpha_1\rho}\right)dx \\ &= \int_0^\infty \left(\frac{\left|H_e^{LoS}\right|^2}{\delta_{nle}^2}+1\right)\exp\left[-\left(\frac{\left|H_e^{LoS}\right|^2}{\delta_{nle}^2}+\left(\frac{\left|H_e^{LoS}\right|^2}{\delta_{nle}^2}+1\right)x\right)\right]* \\ &I_0\left(2\sqrt{x*\frac{\left|H_e^{LoS}\right|^2}{\delta_{nle}^2}\left(\frac{\left|H_e^{LoS}\right|^2}{\delta_{nle}^2}+1\right)}\right)* \\ &\left[1-Q_1\left(\sqrt{2\frac{\left|H_2^{LoS}\right|^2}{\delta_{nl2}^2}},\sqrt{2\left(1+\frac{\left|H_2^{LoS}\right|^2}{\delta_{nl2}^2}\right)}*\sqrt{\frac{2^{\widetilde{R_{s2}}}(1+\alpha_2\rho x)-1}{(\alpha_1+\alpha_2)\rho-2^{\widetilde{R_{s2}}}(1+\alpha_2\rho x)\alpha_1\rho}}\right)\right]dx \end{aligned} \tag{37}$$

where $\delta_{nle}^2 = \frac{M\times h_0^2\times d_{b,r}^{-\alpha}\times d_{r,e}^{-\beta}(R_1+R_{2,e}+1)}{(R_1+1)(R_{2,e}+1)}$.

4. Numerical Simulation

4.1. Simulation Parameter Setting

In this section, the user's outage probability and secrecy outage probability are verified and analyzed through MATLAB simulation, and the effects of several important parameters, such as the channels' Rician factor, the number of RIS elements, the pass loss index, the distance, etc., on the performance of the communication system are investigated. The performance enhancement capability of NOMA on the RIS-UAV-assisted communication system is explored by using OMA as a baseline scenario. The simulation is based on the Rician fading environment, considering the small-scale fading and path loss in signal transmission, and the specific simulation parameters are set in Table 1:

Table 1. System Simulation Parameter Setting.

Parameter	Parameter Value
Path loss index from the base station to the RIS-UAV α	2
Path loss index from RIS-UAV to users β	3
Path loss per unit distance h_0	−20 db
User target transmission rate	1 bps/HZ
User power allocation factor	$\alpha_1 = 0.4$ $\alpha_2 = 0.6$
Distance from BS to RIS-UAV center $d_{b,r}$	15 m
RIS-UAV to user 1 distance $d_{r,1}$	20 m
RIS-UAV to User 2 distance $d_{r,2}$	25 m
RIS-UAV to eavesdropper distance $d_{r,e}$	50 m

4.2. Analysis of Numerical Simulation Results

Figure 3a,b give the effects of different Rician factors on the outage probability of two users under different transmitting SNRs when the RIS element is 300, U_1 power allocation $\alpha_1 = 0.4$, and U_2 power allocation $\alpha_2 = 0.6$. Overall, since the UAV equipped with RIS is far away from the base station as well as the users, the power is not enough to support the normal information transmission of the communication system before the transmitting SNR reaches a certain threshold, and at this time, the users' outage probability is 1. After arriving at the threshold, the user's outage probability decreases with the increase in the transmitting SNR. From the impact of Rician factor on the outage probability, since the size of Rician factor represents the component share of the LoS link in information transmission, the larger the Rician factor, the smaller its outage probability; when the Rician factor is 0, the channel is degraded from a Rician fading environment to a Rayleigh fading, and the numerical simulation shows that the outage probability of the Rician channel is lower compared with that of the Rayleigh channel. For two users, it can be seen that U_1 is a near user with better channel conditions and U_2 is a far user with poorer channel conditions, so in the longitudinal comparison, the outage probability of U_1 is smaller than that of U_2 in the case of the same transmitting SNR.

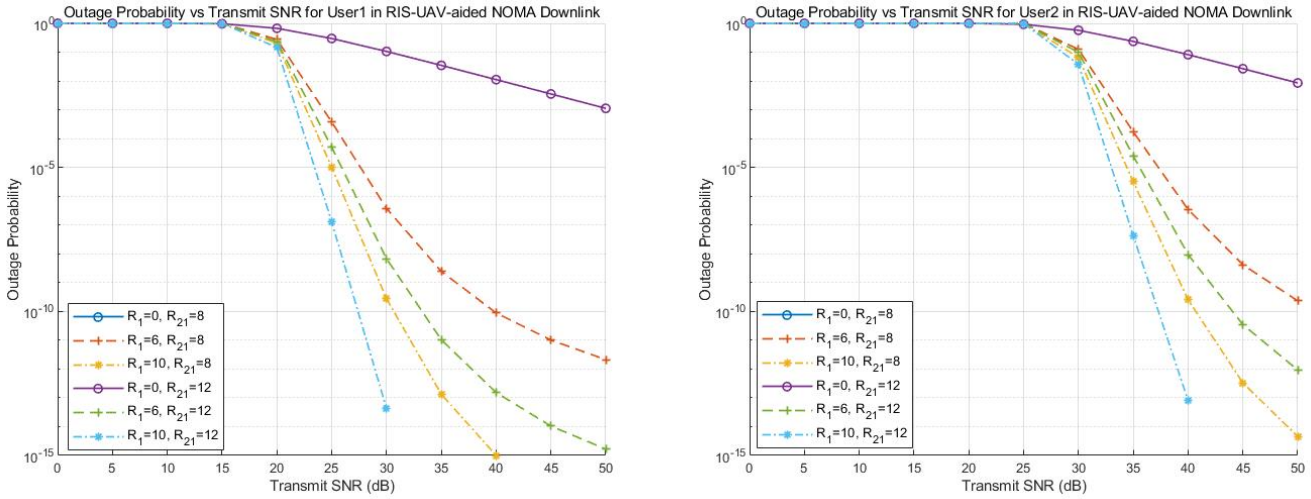

(**a**) (**b**)

Figure 3. (**a**) Effect of Rician factor on outage probability for different transmitting SNR for user 1; (**b**) Effect of Rician factor on outage probability for different transmitting SNR for user 2.

Figure 4a,b reveal the outage probability of the NOMA users under different path loss indices. It can be seen that the greater the path loss index, the greater the outage probability of the user. When the transmit SNR reaches a certain threshold, the degree of influence of the path loss is weakened. Figure 5a,b show the influence of the distance $d_{b,r}, d_{r,1}, d_{r,2}$ on the user's outage probability. When the transmitting SNR is less than a certain threshold, the user outage probability increases with the increase in the distance. When the transmitting SNR reaches a certain threshold, the user's outage probability is related to the size of the two distance parameters. When the RIS-UAV is closer to the base station, the outage probability is smaller. Therefore, in practical applications, the position of the RIS-UAV can be considered closer to the base station.

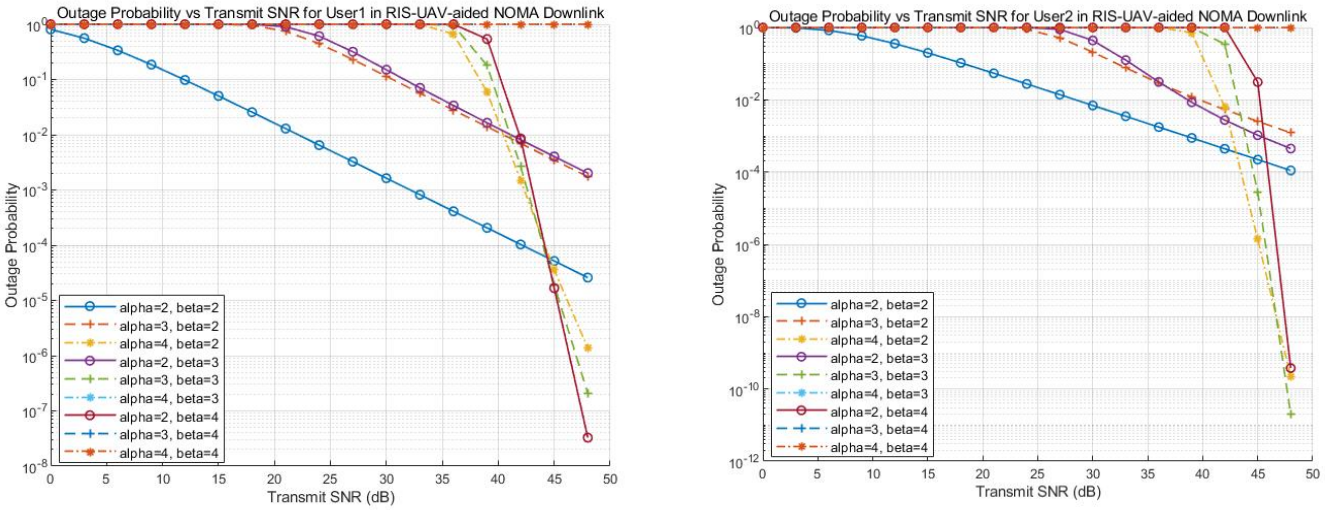

(**a**) (**b**)

Figure 4. (**a**) Outage probability of user 1 under different path loss indices; (**b**) Outage probability of user 2 under different path loss indices.

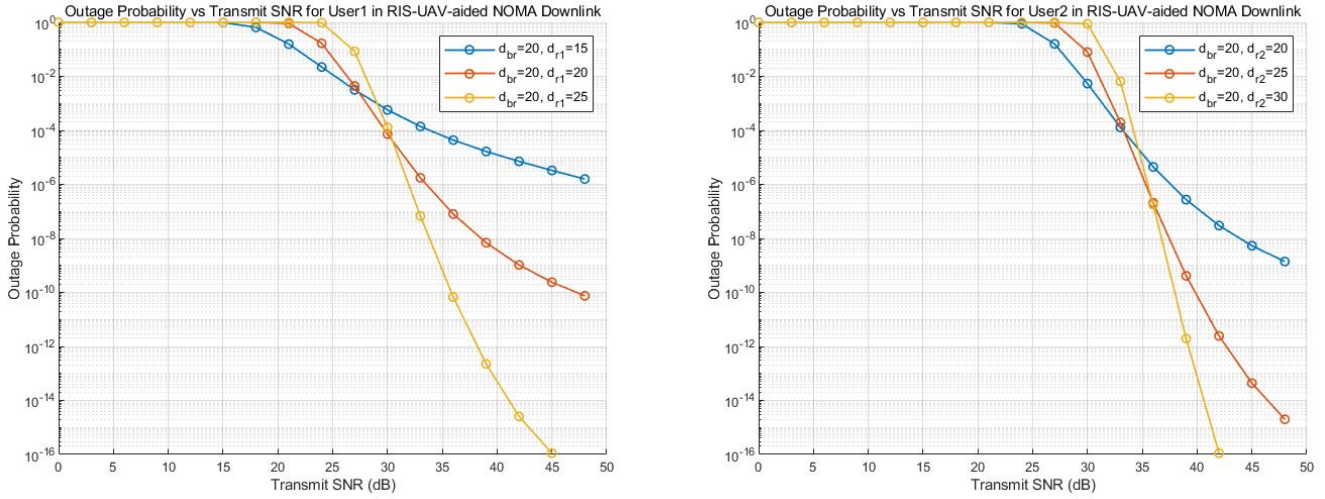

(**a**) (**b**)

Figure 5. (**a**) Outage probability of user 1 under different distances; (**b**) Outage probability of user 2 under different distances.

Figure 6 explores the effect of the number of RIS elements and the NOMA power allocation factor on the user's outage probability. The numerical results show that the increase in the number of RIS elements can effectively reduce the outage probability, and the user's outage probability also decreases with the increase in the allocated power. In addition, it is found that the effect of the RIS elements on the outage probability is more pronounced than the size of the power allocation, which is reflected in curves 4 and 5 in Figure 6, where the outage probability of the user is lower than that of the case of $M = 300$ and $\alpha_1 = 0.4$, when $M = 400$ and $\alpha_1 = 0.2$. Figure 7 gives the outage probability of two users in OMA and NOMA modes when $\alpha_1 = 0.15$ and $\alpha_2 = 0.85$, and numerically verifies that the outage probability of the user will be lower in the NOMA mechanism. In this case, the outage probability of user 2 is lower because more power is allocated to user 2.

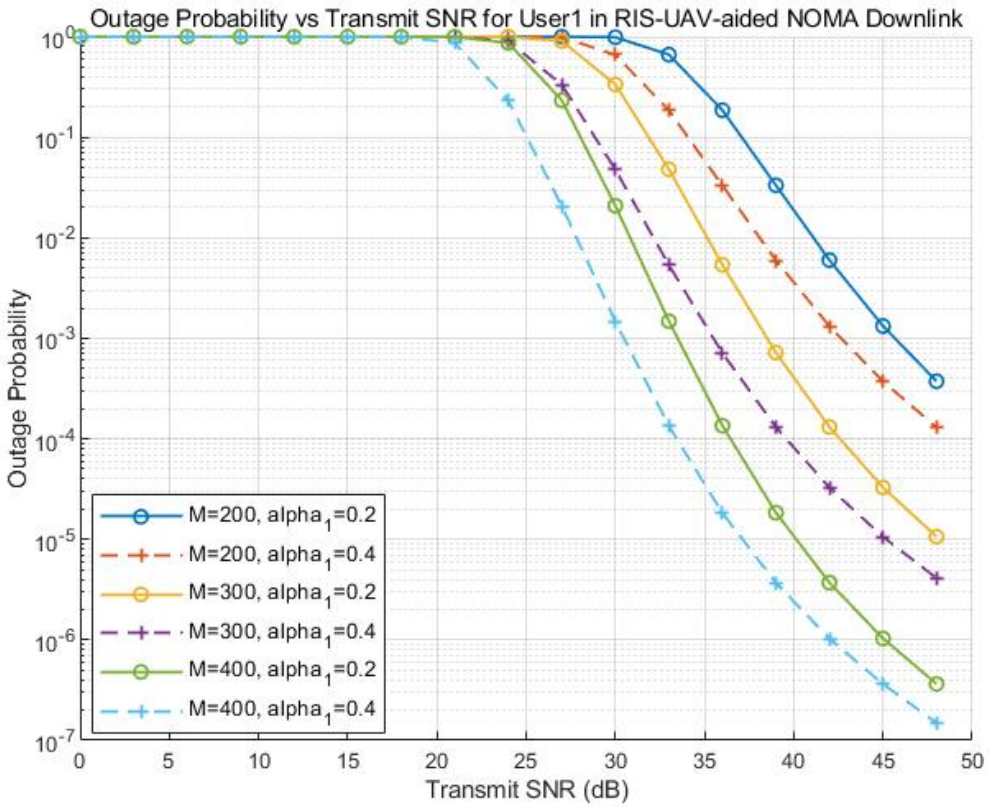

Figure 6. Effect of different numbers of RIS elements and user power allocation factor on user 1 outage probability.

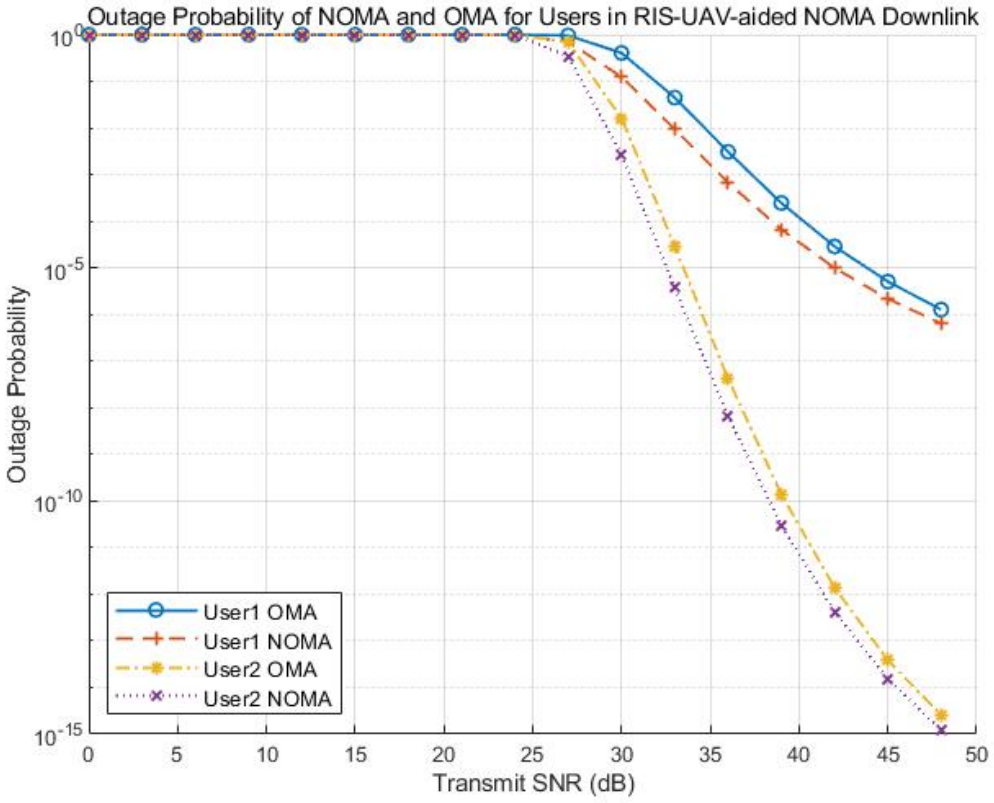

Figure 7. Users' outage probability in OMA and NOMA transmission modes.

Figure 8 gives the security outage probability when the target security rate of user 1 is 0.04. It is numerically verified that the number of RIS elements and the power allocation factor of the user are negatively correlated with its security outage probability. The secure communication performance of the user improves with the increase in the number of RIS elements and the power allocation, which is manifested by the decrease in its outage probability. When the transmitting SNR reaches a certain level, the allocation of a larger power can make up for the insufficiency of the number of RIS elements, which is manifested by the fact that the outage probability of the number of RIS elements of 1000 and the power allocation factor of 0.4 is higher than that of when the SNR reaches 25, the outage probability of RIS elements of 1000 with a power allocation factor of 0.4 is smaller than that of RIS elements of 800 with a power allocation factor of 0.2. This finding provides a basis for thinking about the next step of the joint optimization of the power allocation and the RIS settings.

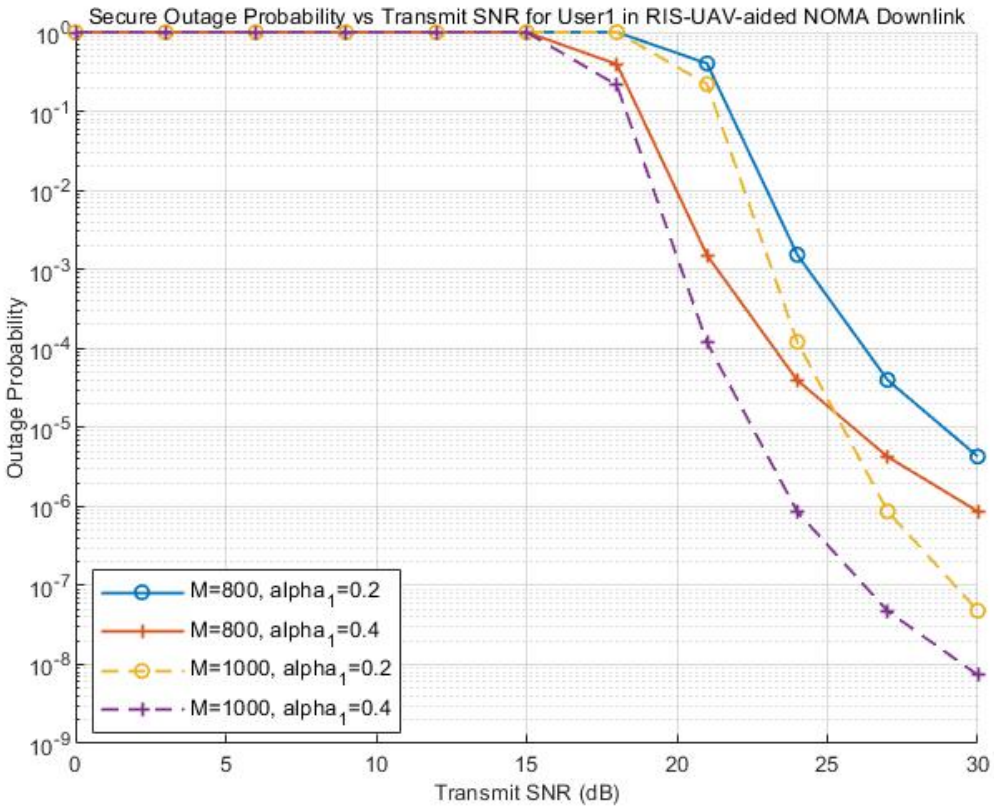

Figure 8. Effect of the RIS element number and power allocation factor on secrecy outage probability of the user 1.

Figures 9 and 10 give the effect of different Rician factors on the user's security outage probability as well as the user's information transmission SOP in NOMA transmission mode and OMA mode, respectively. For U_1, it is also verified that the Rician channel as well as the NOMA transmission mode are effective in acting on the communication security of the system. Figure 9 shows that when the Rician factor is 0, the channel is degraded from Rician fading to Rayleigh fading channel, and the numerical simulation verifies that the user's security outage probability is higher when the channel from the base station to the RIS-UAV is a Rayleigh channel. Secondly, as the Rician factor increases, the user's SOP is greater, which is due to the enhancement of the signal of the direct link, and the legitimate user receives a better signal, but due to the distance of the legitimate user is farther away, so the eavesdropping effect will be worse in comparison. Figure 10 then shows that NOMA demonstrates a lower probability of security disruption for user 1's secure transmission compared to the OMA transmission mode.

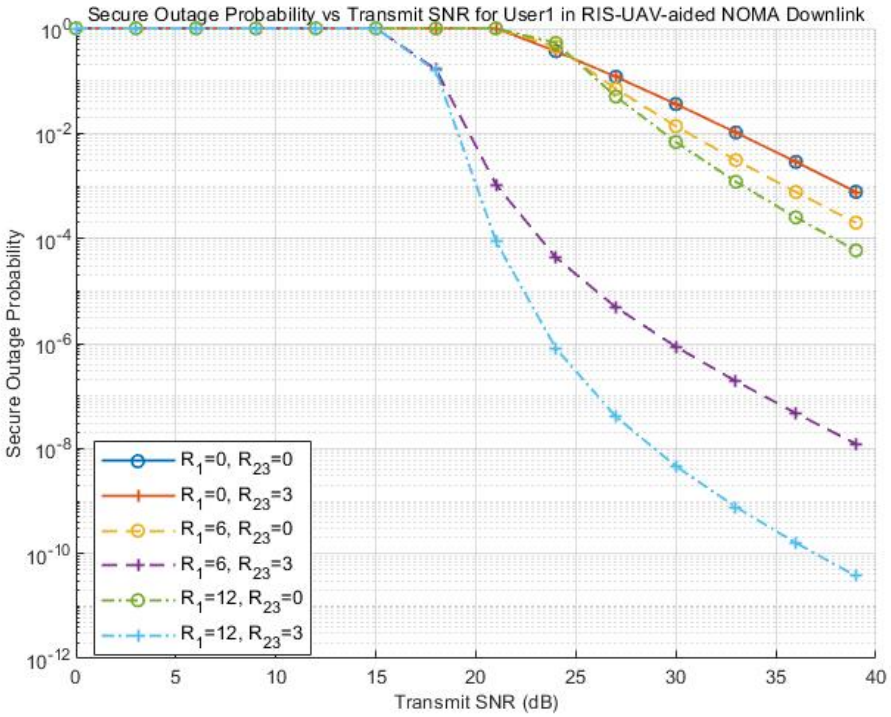

Figure 9. Effect of the Rician factor on the secrecy outage probability of the user 1.

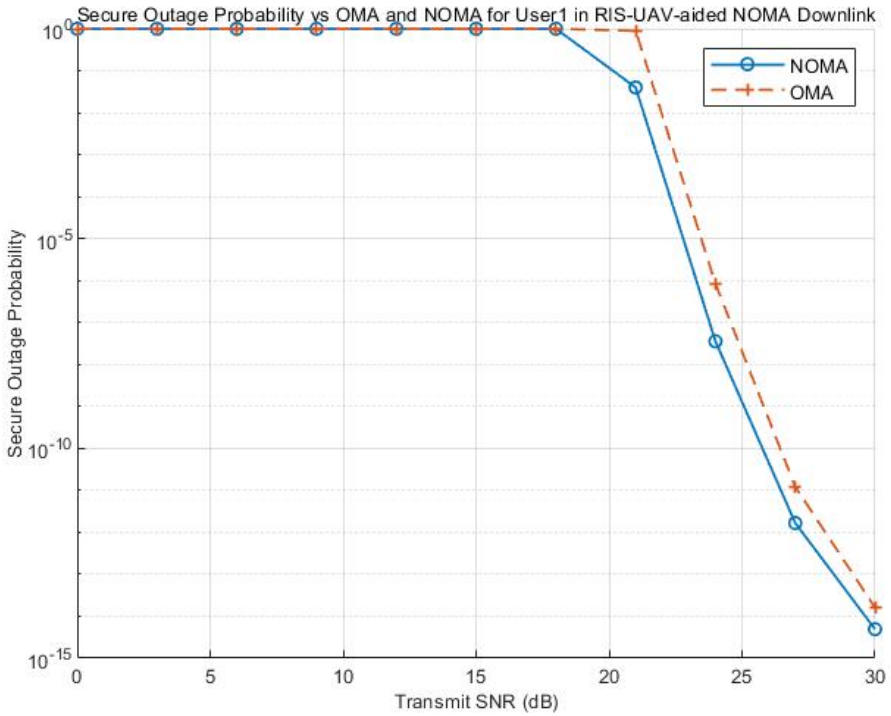

Figure 10. Comparison of the secrecy outage probability of user 1 in NOMA and OMA modes.

5. Conclusions

Due to the ground obstacles and limited onboard battery power, while UAV-assisted aerial communication has advantages such as flexible deployment and wide coverage, energy issues need to be considered. Given the high energy efficiency advantages of reconfigurable intelligent surfaces in improving wireless channel propagation environments, a RIS-UAV-assisted NOMA downlink communication system is proposed in this paper, and in view of the LoS environment of the Air-to-Ground link, the Rician fading scenario,

which is more relevant to the actual channel, is chosen for the study. The outage probability of the system's NOMA users is investigated by approximating the composite channel as an overall Rician distribution, and the user's secrecy outage probability is further investigated by considering the physical layer security in the presence of the eavesdropper. Numerical simulation results verify that, compared with the Rayleigh fading scenario, Rician fading can provide a better link environment for signal transmission due to the presence of LoS links, and the user's outage probability is lower; increasing the number of RIS elements can effectively reduce the system's outage probability; and the application of the NOMA technique can likewise improve the system's communication performance.

Since UAV communication faces problems such as energy limitation and safety in assisting disaster response and combat scenarios, RIS mounted on UAVs can effectively improve the performance and safety of the communication system. Considering the Rician channels fading environment, which is more practical with the actual links, the NOMA system proposed in this paper has been verified to have better communication performance than Rayleigh channels and can perform active power allocation and RIS element number arrangement according to the information receiving requirements of legitimate users. In practical applications, the introduction of RIS attached to the UAV for auxiliary communication can effectively improve the onboard energy-limited problem and significantly improve the performance of the NOMA communication system by intelligently adjusting the wireless signal propagation path to achieve more efficient spectrum utilization and better signal coverage. In addition, the reconfigurability of RIS provides a more flexible and efficient communication environment for UAV communication, improving the auxiliary communication capability and the application development of NOMA technology in the field of secure communication. In future work, we will also consider popular research directions such as multi-function drones, conformal RIS, terahertz (THz) channels, joint optimization, and so on to explore more efficient and available methods for 6G development and UAV applications.

Author Contributions: X.L. researched the literature, provided the mathematical models, designed the algorithm, completed numerical simulations, took charge of the original draft preparation, and edited the manuscript; S.L. conceived the study concepts, improved the systematic research and analysis methodology, and supervised the completion of the refinement of the paper; J.G. and G.P. gave valuable suggestions for revision, checked formula deducing, and English grammar. All authors have read and agreed to the published version of the manuscript.

Funding: This research was funded in part by the National Natural Science Foundation of China (62467004) and in part by the Hongliu First Class Discipline Development Project of Lanzhou University of Technology (25-225305).

Data Availability Statement: The data supporting this article are from previously reported studies and datasets, which have been cited.

Conflicts of Interest: The authors declare no conflicts of interest.

References

1. China Center for Information Industry Development. *White Paper on 6G Concepts and Vision*; CCID Think Tank: Beijing, China, 2020; p. 14.
2. Sharif, S.; Liaq, M.; Ejaz, W. Multi-objective resource optimization in Space-Aerial-Ground-Sea integrated networks. In Proceedings of the 2023 IEEE Symposium on Wireless Technology & Applications (ISWTA), Kuala Lumpur, Malaysia, 15–16 August 2023; pp. 109–114.
3. Sharif, S.; Zeadally, S.; Ejaz, W. Space-aerial-ground-sea integrated networks: Resource optimization and challenges in 6G. *J. Netw. Comput. Appl.* **2023**, *215*, 103647. [CrossRef]
4. Daurembekova, D.; Schotten, H.D. Opportunities and limitations of Space-Air-Ground integrated network in 6G systems. In Proceedings of the 2023 IEEE 34th Annual International Symposium on Personal, Indoor and Mobile Radio Communications (PIMRC), Toronto, ON, Canada, 5–8 September 2023; pp. 1–7.
5. Kang, J.; Kim, K.; Lee, H.; Kim, J.H. Lyapunov optimization-based online positioning in UAV-assisted emergency communications. *IEEE Access* **2023**, *11*, 60835–60843. [CrossRef]

6. Xu, C.; Jiang, Y. Enhance broadcasting throughput by associating network coding with UAVs relays deployment in emergency communications. In Proceedings of the 19th EAI International Conference on Collaborative Computing: Networking, Applications and Worksharing, Corfu Island, Greece, 4–6 October 2023; pp. 173–190.
7. Sara, F.; Engy, M.; Ahmed, E.M.; Falko, D. Performance analysis of UAV assisted mobile communications in THz channel. *IEEE Access* **2021**, *9*, 160104–160115.
8. Wu, Q.; Zhang, S.; Zheng, B.; You, C.; Zhang, R. Intelligent reflecting surface-aided wireless communications: A tutorial. *IEEE Trans. Commun.* **2021**, *69*, 3313–3351. [CrossRef]
9. Liu, Y.; Liu, X.; Mu, X.; Hou, T.; Xu, J.; Di Renzo, M.; Al-Dhahir, N. Reconfigurable intelligent surfaces: Principles and opportunities. *IEEE Commun. Surv. Tutor.* **2021**, *23*, 1546–15778. [CrossRef]
10. Yuan, Q.; Hu, Y.; Wang, C.; Li, Y. Joint 3D beamforming and trajectory design for UAV-enabled mobile relaying system. *IEEE Access* **2019**, *7*, 26488–26496. [CrossRef]
11. Song, Q.; Zheng, F.; Zeng, Y.; Zhang, J. Joint beamforming and power allocation for UAV-enabled full-duplex relay. *IEEE Trans. Veh. Technol.* **2019**, *68*, 1657–1671. [CrossRef]
12. Abdullah, Z.; Chen, G.; Lambotharan, S.; Chambers, J.A. A hybrid relay and intelligent reflecting surface network and its ergodic performance analysis. *IEEE Wirel. Commun. Lett.* **2020**, *9*, 1653–1657. [CrossRef]
13. Atapattu, S.; Fan, R.; Dharmawansa, P.; Wang, G.; Evans, J.S.; Tsiftsis, T.A. Reconfigurable intelligent surface assisted two-way communications: Performance analysis and optimization. *IEEE Trans. Commun.* **2020**, *68*, 6552–6567. [CrossRef]
14. Xu, P.; Chen, G.; Pan, G.; Di Renzo, M. Ergodic secrecy rate of RIS-assisted communication systems in the presence of discrete phase shifts and multiple eavesdroppers. *IEEE Wirel. Commun. Lett.* **2020**, *10*, 629–633. [CrossRef]
15. Sánchez, J.D.V.; Ramírez-Espinosa, P.; López-Martínez, F.J. Physical layer security of large reflecting surface aided communications with phase errors. *IEEE Wirel. Commun. Lett.* **2020**, *10*, 325–329. [CrossRef]
16. Xu, P.; Chen, G.; Yang, Z.; Di Renzo, M. Reconfigurable intelligent surfaces-assisted communications with discrete phase shifts: How many quantization levels are required to achieve full diversity. *IEEE Wirel. Commun. Lett.* **2020**, *10*, 358–362. [CrossRef]
17. Tao, Q.; Wang, J.; Zhong, C. Performance analysis of intelligent reflecting surface aided communication systems. *IEEE Commun. Lett.* **2020**, *24*, 2464–2468. [CrossRef]
18. Salhab, A.M.; Samuh, M.H. Accurate performance analysis of reconfigurable intelligent surfaces over Rician fading channels. *IEEE Wirel. Commun. Lett.* **2021**, *10*, 1051–1055. [CrossRef]
19. Zhang, H.; Di, B.; Song, L.; Han, Z. Reconfigurable intelligent surfaces assisted communications with limited phase shifts: How many phase shifts are enough? *IEEE Trans. Veh. Technol.* **2020**, *69*, 4498–4502. [CrossRef]
20. Li, D. Ergodic capacity of intelligent reflecting surface-assisted communication systems with phase errors. *IEEE Commun. Lett.* **2020**, *24*, 1646–1650. [CrossRef]
21. Diao, D.; Wang, B.; Cao, K.; Weng, J.; Dong, R.; Cheng, T. Secure wireless-powered NOMA communications in multi-UAV systems. *IEEE Trans. Green Commun. Netw.* **2023**, *7*, 1205–1216. [CrossRef]
22. Zhang, Y.; Wang, H.M.; Yang, Q.; Ding, Z. Secrecy sum rate maximization in non- orthogonal multiple access. *IEEE Commun. Lett.* **2016**, *20*, 930–933. [CrossRef]
23. Liu, Y.; Qin, Z.; Elkashlan, M.; Gao, Y.; Hanzo, L. Enhancing the physical layer security of non-orthogonal multiple access in large-scale networks. *IEEE Trans. Wirel. Commun.* **2017**, *16*, 1656–1672. [CrossRef]
24. Huang, S.; Xiao, M.; Poor, H.V. On the physical layer security of millimeter wave NOMA networks. *IEEE Trans. Veh. Technol.* **2020**, *69*, 11697–11711. [CrossRef]
25. Pei, Y.; Yue, X.; Yi, W.; Liu, Y.; Li, X.; Ding, Z. Secrecy outage probability analysis for downlink RIS-NOMA networks with On-Off control. *IEEE Trans. Veh. Technol.* **2023**, *72*, 11772–11786. [CrossRef]
26. Hou, T.; Liu, Y.; Song, Z.; Sun, X.; Chen, Y.; Hanzo, L. Reconfigurable intelligent surface aided NOMA networks. *IEEE J. Sel. Areas Commun.* **2020**, *38*, 2575–2588. [CrossRef]
27. Zheng, Y.; Yang, S.; Fu, H.; Chen, T. Secure outage probability analysis of relay networks based on cooperative jamming. In Proceedings of the 2018 International Conference on Cyber-Enabled Distributed Computing and Knowledge Discovery (Cyber C), Zhengzhou, China, 18–20 October 2018; pp. 55–553.
28. Wang, D.; Zhao, Y.; Lou, Y.; Pang, L.; He, Y.; Zhang, D. Secure NOMA based RIS-UAV networks: Passive beamforming and location optimization. In Proceedings of the GLOBECOM 2022—2022 IEEE Global Communications Conference, Rio de Janeiro, Brazil, 4–8 December 2022; pp. 3168–3173.
29. Yang, F.; Guo, W.; Dai, J. Artificial Noise Aided Secure Transmission for Active RIS-Aided NOMA Networks. *IEEE Access* **2023**, *11*, 78111–78118. [CrossRef]
30. Yue, X.; Xie, J.; Liu, Y.; Han, Z.; Liu, R.; Ding, Z. Simultaneously transmitting and reflecting reconfigurable intelligent surface assisted NOMA networks. *IEEE Trans. Wirel. Commun.* **2023**, *22*, 189–204. [CrossRef]